International Journal of Engineering and Technology Innovation, vol. 16, no. 3, 2026, pp. 370-380

Stability Assessment of Levees under Cyclic Water Level Fluctuations: A Case Study of Princeville Levee

Chan-Jin Jeong, Su-Min Song, Yoon-Seo Lee, Seung-Oh Lee*

Department of Civil and Environmental Engineering, Hongik University, Seoul, South Korea

Received 15 February 2026; revised 18 May 2026; accepted 21 May 2026

DOI: https://doi.org/10.46604/ijeti.2026.16181

Abstract

The increasing frequency of floods threatens levee structural integrity, yet traditional assessments fail to capture history-dependent cumulative damage. This study aims to investigate the progressive hydro-mechanical degradation of the Princeville Levee under 15 cyclic flood events using a fully coupled transient seepage-deformation analysis. Using the strength reduction method, the global factor of safety (FoS) is evaluated at 2.46 during the critical drawdown stage. Although this macroscopic metric exceeds conventional design criteria, implying high stability, our analysis reveals a physical paradox. Due to delayed drainage, the internal soil skeleton undergoes continuous unrecoverable plastic deformation, with peak deviatoric shear strain rising by approximately 15% across cycles. This irreversible ratcheting and stiffness degradation demonstrate that static FoS metrics overestimate long-term stability by masking underlying damage. Ultimately, ensuring aging levee resilience requires a paradigm shift from traditional limit equilibrium approaches to deformation-based serviceability assessments.

Keywords: levee stability, transient seepage, cyclic water level fluctuation, accumulated shear strain, strength reduction method (SRM)

1. Introduction

Levees constructed along rivers are earthen structures designed to protect lowlands from flooding and maintain stable channel flow. To function effectively even under extreme conditions, these levees must possess sufficient structural stability. However, recent climate change has increased the frequency and intensity of floods, resulting in a growing number of levee failures. Levee failure can occur through various mechanisms, with the primary causes including overtopping, erosion, seepage, and slope instability. Overtopping occurs when the water level exceeds the levee crest elevation, while erosion happens when the slope lacks sufficient resistance against hydraulic loads. Internal erosion weakens the structure as soil particles migrate due to seepage flow, forming voids within the embankment. Slope instability is caused by a reduction in shear strength due to increased pore water pressure, and rapid water level fluctuations are considered one of the major contributing factors [1].

Historically, levee failures were predominantly caused by overtopping. However, as levees have been reinforced, seepage failure due to the complex interaction between rainfall and river water levels has emerged as an increasingly critical concern [2]. Seepage generally refers to the outflow of infiltrating water at the landside toe of the levee, occurring when rising river water penetrates the embankment. When the phreatic line reaches the landside slope, leakage occurs, which can induce piping phenomena and pose a significant risk of levee collapse. This seepage process critically affects the overall stability of earthen structures such as levees.

* Corresponding author. E-mail address: seungoh.lee@hongik.ac.kr

Experimental approaches have been employed to understand these phenomena. Park et al. [3] conducted seepage analysis using time domain reflectometry (TDR) sensors and identified changes in the phreatic line over time by distinguishing between saturated, unsaturated, and dry zones through hydraulic model tests. Jin et al. [4] performed centrifuge model tests on reinforced levees, analyzing seepage behavior and the expansion of saturated zones based on reinforcement location and foundation conditions. While such physical model tests provide a fundamental understanding of seepage behavior, they are limited in their ability to perform precise internal analysis due to temporal and spatial constraints.

Consequently, the stability assessment of levees regarding seepage is widely conducted using numerical analysis methods. Numerical seepage analysis can simulate internal behaviors that are difficult to capture through experiments or field monitoring, allowing for the proactive evaluation of risk factors. In particular, transient seepage analysis is emphasized for its ability to incorporate time-dependent boundary and loading conditions. This enables a more realistic evaluation of pore water pressure and stability inside the levee during floods. While steady-state analysis assumes a constant water level, it often results in excessive pore water pressures and conservatively low safety factors. In contrast, transient analysis reflects the actual process of water-level changes, enabling a more accurate stability assessment [5].

Stability assessment of embankment structures has historically relied on two primary approaches, namely the limit equilibrium method (LEM) and the strength reduction method (SRM) [6-9]. While LEM remains widely used due to its simplicity and established practice, it exhibits critical limitations when assessing levees subjected to cyclic hydraulic loading [10-11].

The method relies on a rigid-plastic assumption and considers only force or moment equilibrium on a potential slip surface. This approach does not adequately represent the stress-strain behavior of the soil. Consequently, LEM fails to account for stiffness degradation and the cumulative shear strain that occurs during repeated water level fluctuations. It further assumes that soil strength remains constant regardless of the deformation history.

To overcome these deficiencies, the SRM is adopted in this study. SRM is typically implemented within a finite element framework and can explicitly incorporate the stress-strain relationship of the soil material. This allows for the simulation of plastic deformation accumulation and the progressive reduction in stability induced by cyclic seepage forces. Previous research supports the necessity of this deformation-based approach. For instance, Jadid et al. [12] demonstrated that under cyclic water level changes, shear strain within a levee can increase by up to 3.5 times as the number of cycles increases. This accumulation gradually increases the probability of exceeding the performance limit state. Therefore, unlike LEM, SRM can visualize the development of failure mechanisms over time and provides a more rigorous evaluation of levee safety under complex hydraulic loading conditions.

Recent studies have addressed the impact of water level fluctuations resulting from extreme climate conditions on the hydro-mechanical stability of levees. Sun et al. [13] numerically demonstrated the effect of the water level drawdown rate on the transient seepage field and slope instability, while Kim et al. [14] evaluated the instability mechanism of slopes occurring under alternating rapid water level rise and drawdown conditions. In addition, Janssen et al. [15] experimentally confirmed that transient water infiltration gradually raises the phreatic line, severely reducing shear resistance. However, existing literature tends to focus mainly on single flood events or simple water level drawdown scenarios, thus failing to adequately reflect the cumulative deformation and irreversible stiffness degradation of soil caused by repetitive flood cycles.

Therefore, this study aims to quantitatively analyze seepage behavior and stability changes of levees under cyclic water level conditions through numerical transient seepage analysis. Specifically, this study evaluates the accumulation of shear strain and the potential for exceeding performance limit states under cyclic seepage loads using the SRM. The findings are expected to provide a more reliable basis for levee stability assessment under repetitive flood conditions.

2. Study Area

The Princeville Levee is located in Princeville, Edgecombe County, North Carolina, encompassing the western, southwestern, and northern boundaries of the town along the Tar River. Historically known as “Freedom Hill,” Princeville holds national significance as the first town in the United States incorporated by freed slaves in 1885. Despite its historical value, the town’s low-lying topography has made it highly susceptible to flooding.

The existing levee was constructed by the U.S. Army Corps of Engineers (USACE) in 1967 under the Flood Control Act of 1948 to mitigate these risks. The design was originally based on the flood of 1919, which was considered a 300-year event at the time. However, recent climate change has increasingly challenged the performance of this infrastructure.

Most notably, Hurricane Floyd in 1999 produced a catastrophic flood event exceeding the 500-year recurrence interval. During this event, the hydraulic load exceeded the levee’s capacity, causing the Tar River to bypass and overtop the levee. The resulting inundation was devastating. Flood depth rose up to 6 meters and submerged buildings to their rooftops. The town remained completely flooded for eleven days before the floodwaters receded. This prolonged submersion caused extensive destruction to residential and commercial properties. The geographical alignment of the levee and the extent of historical flood damage are illustrated in Fig. 1. Specifically, Fig. 1(a) shows the satellite map of the levee alignment, while Fig. 1(b) depicts the severe inundation caused by Hurricane Floyd in 1999.

(a) Satellite map showing the alignment of the Princeville Levee along the Tar River

(b) Aerial view of severe inundation during Hurricane Floyd in September 1999

Fig. 1 Location and historical flood damage of the study area [17]

Following this disaster, the levee was restored in 2000, and Executive Order 13146 was issued to mandate federal assistance for the protection of the town. However, the recurrence of extreme hydraulic loading, such as Hurricane Matthew in 2016, continues to threaten the integrity of the levee system. These historical events demonstrate that the levee is subjected to recurrent and prolonged hydraulic stresses, underscoring the critical necessity of stability analyses that account for cyclic water level fluctuations and seepage-induced deformation [16].

To evaluate the stability of the levee under the most critical conditions, this study focuses on Station 74+00. According to a fragility analysis conducted by USACE [17], this section exhibited the highest probability of failure among the analyzed reaches. Consequently, Station 74+00 was selected as the representative model for the numerical seepage and stability analysis. The geometry of the selected cross-section is illustrated in Fig. 2. The levee has a height of approximately 9.0 m and a bottom width of 67.5 m. The slope gradients are designed as 1V:3H on the riverside and 1V:2.5H on the landside. The stratigraphic profile reveals a complex, heterogeneous soil composition classified according to the Unified Soil Classification System (USCS). As shown in Fig. 2, the levee body primarily consists of clayey sand (SC). Notably, layers of lean clay (CL) are interbedded horizontally within the embankment to create a stratified structure. This layering is critical for seepage analysis because the lower-permeability clay layers may induce anisotropy in hydraulic conductivity. This potentially impedes vertical flow and alters the development of the phreatic surface.

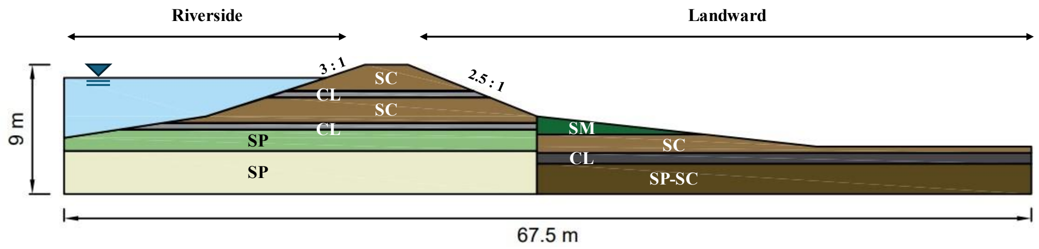

Fig. 2 Princeville levee cross section (station 74 + 00)

The foundation soil exhibits distinct characteristics on either side of the levee centerline. The riverside foundation is predominantly composed of poorly graded sand (SP). In contrast, the landside foundation consists of a complex mixture of silty sand (SM), SC, and CL. To accurately simulate the unsaturated flow behavior within these soils, specific soil water characteristic curves (SWCC) were assigned to each soil type in the numerical model. For this purpose, the van Genuchten model was adopted. The specific curve fitting parameters, including residual water content (θ_r) saturated water content (θ_s), air entry parameter (a), and pore size distribution index (n), were determined based on the United States Department of Agriculture (USDA) soil classification system and the widely used database proposed by Carsel and Parrish [18]. The detailed parameters assigned to each soil layer are summarized in Table 1.

Table 1 Properties of soil and its consolidation characteristics

Soil Parameters	SC	SP	CL	SM	SP-SC
$\gamma(kN/m^3)$	19.6	18.9	20.7	19.6	18.9
c'(kPa)	3.6	0	144	0	0
φ'(°)	30	28	0	33	28
E_{50}^{ref}(kPa)	4.07×10^4	4.07×10^4	4.07×10^4	4.07×10^4	4.07×10^4
E_{oed}^{ref}(kPa)	4.07×10^4	4.07×10^4	4.07×10^4	4.07×10^4	4.07×10^4
E_{ur}^{ref}(kPa)	4.07×10^4	4.07×10^4	4.07×10^4	4.07×10^4	4.07×10^4
$k(m/day)$	0.288	7.13	0.0475	3.50	1.06
θ_r(-)	0.100	0.045	0.068	0.057	0.065
θ_s(-)	0.38	0.43	0.38	0.41	0.41
$a(1/m)$	2.7	14.5	0.8	12.4	7.5
n(-)	1.23	2.68	1.09	2.28	1.89

The unit weight (γ), strength parameters (c', φ'), and hydraulic conductivity (k) values were originally derived from the site-specific investigation data reported by USACE (2015) [17]. Due to the lack of specific laboratory test data for the stiffness parameters, the reference moduli for the hardening soil model (E_{50}^{ref}, E_{oed}^{ref} and E_{ur}^{ref}) were selected based on well-established empirical correlations and literature-based data presented in the foundational study by Schanz et al. [19].

3. Numerical Modeling Methods

To quantitatively evaluate the progressive degradation and long-term stability of the levee under cyclic environmental actions, a comprehensive numerical simulation workflow was established. This section describes the governing equations, material behavior, and spatial-temporal discretization utilized in the finite element analysis.

3.1 Fully Coupled Hydro-Mechanical Framework

In this study, the finite element software PLAXIS 2D was used to analyze the deformation behavior of the levee under transient seepage and cyclic water level fluctuations. The analysis was conducted under the plane strain condition, assuming that the cross-section remains consistent along the longitudinal axis.

Conventionally, many numerical codes widely employed for seepage and stability assessment (e.g., SEEP/W and Slide2) adopt a decoupled approach. In this method, pore water pressure distributions are calculated independently and subsequently imported into a limit equilibrium or separate stress analysis module to assess stability. However, such a framework has limitations in capturing the simultaneous hydro-mechanical coupling. It often neglects the real-time interaction between transient seepage forces, effective stress redistribution, and the soil skeleton deformation. The interaction between soil deformation and pore fluid flow is governed by the mechanical equilibrium condition, as expressed below:

$$\nabla \cdot \sigma' + \rho g = 0 \tag{1}$$

where σ' represents the effective stress tensor, ρ denotes the density of the material, and g signifies the gravitational acceleration vector. The critical link between this mechanical equilibrium and the hydraulic flow is established through the effective stress principle. The effective stress σ' is not a constant but is dependent on the pore water pressure (p_w), as defined by Bishop's effective stress concept for unsaturated soils:

$$\sigma' = (\sigma - u_a) + \chi(u_a - p_w) \tag{2}$$

where σ is the total stress. u_a is the pore air pressure, and χ is the effective stress parameter related to the degree of saturation. Importantly, the pore water pressure (p_w) in this equation is directly derived from the transient seepage analysis.

This equation ensures that the internal stresses, pore pressures, and external body forces maintain a state of equilibrium throughout the analysis domain. For the transient seepage behavior in unsaturated soils, the analysis employed Richards' equation, which governs the flow of water in a porous medium, as defined as:

$$\frac{\partial \theta}{\partial t} = \nabla \cdot \left[k(\psi) \nabla (h + z) \right] \tag{3}$$

where θ represents the volumetric water content and t denotes time. The term $k(\psi)$ refers to the hydraulic conductivity as a function of the matric suction ψ, while h and z correspond to the pressure head and elevation head, respectively.

Notably, the pressure head h is directly defined by the pore water pressure (p_w) as $p = p_w/\gamma_w$. Therefore, solving Eq. (3) yields the pressure head h. This is immediately converted to p_w to update the effective stress in Eq. (2), thereby including deformation in Eq. (1). Additionally, the term $k(\psi)$ refers to the hydraulic conductivity dependent on the matric suction $\psi(= u_a - p_w)$. Since matric suction is defined as the difference between pore air and water pressures, the hydraulic properties are also intrinsically linked to the pore water pressure calculated in this step.

To close the system of equations, the hydraulic properties are defined using the van Genuchten [20] model. The relationships for the effective degree of saturation (S_e) and the relative hydraulic conductivity k_r can be expressed as follows:

$$S_e = \frac{\theta - \theta_r}{\theta_s - \theta_r} = \left[1 + \left(\alpha |\psi| \right)^n \right]^{-m} \tag{4}$$

$$k(\psi) = k_{sat} S_e^l \left[1 - \left(1 - S_e^{1/m} \right)^m \right]^2 \tag{5}$$

where θ_s and θ_r are the saturated and residual volumetric water contents, respectively, and k_{sat} is the saturated hydraulic conductivity. The parameters α, n, and $m(m = 1 - 1/n)$ are fitting parameters related to the soil pore structure, while l is a pore connectivity parameter.

3.2 Constitutive Modeling for Cumulative Deformation

The hardening soil (HS) model [19] was employed to accurately simulate the nonlinear behavior of the levee soil under cyclic hydraulic loading. Unlike the linear elastic-perfectly plastic Mohr-Coulomb model, the HS model is an advanced elastoplastic model. It is particularly suitable for reproducing stiffness degradation during shear loading and the expansion of the yield surface due to accumulated plastic strain. Furthermore, it effectively captures the distinct stiffness characteristics exhibited during loading and unloading phases by distinguishing between the secant stiffness (E_{50}) and the unloading-reloading stiffness (E_{ur}). The relationship between the deviatoric stress (q) and the vertical strain (ϵ_1) in the primary loading phase is described by the following hyperbolic function:

$$\varepsilon_1 = \frac{1}{2E_{50}} \times \frac{q}{1-\frac{q}{q_a}},\ for\ q < q_f \tag{6}$$

where q_a represents the asymptotic shear strength and q_f is the ultimate deviatoric stress derived from the Mohr-Coulomb failure criterion. The stiffness of the soil in this model is stress-dependent and is calculated from the reference secant stiffness $\left(E_{50}^{ref}\right)$ as:

$$E_{50} = E_{50}^{ref}\left(\frac{c'\cos\phi' - \sigma_3'\sin\phi'}{c'\cos\phi' + p^{ref}\sin\phi'}\right)^m \tag{7}$$

where E_{50} is the secant stiffness modulus, p^{ref} is the reference pressure, and σ_3' is the minor principal stress. The parameters c' and ϕ' correspond to the effective cohesion and the internal friction angle, respectively. The exponent m controls the level of stress dependency. Similarly, the oedometer stiffness (E_{oed}) and the unloading-reloading stiffness (E_{ur}) obey the same stress-dependent rule as Eq. (7) but use their corresponding reference modulus $\left(E_{oed}^{ref}\ and\ E_{ur}^{ref}\right)$ as listed in Table 1.

3.3 Simulation of Cyclic Hydraulic Loading and Model Setup

The finite element mesh was generated using 15-node triangular elements to ensure high computational precision, as illustrated in Fig. 3. A generally fine mesh was applied throughout the analysis domain to accurately capture the hydraulic and mechanical behavior. Furthermore, local refinement was implemented in critical zones where significant hydraulic gradients and shear strains were anticipated, including the slope surfaces, layer interfaces, and the path of the phreatic surface. The resulting mesh comprised 1,462 elements and 11,989 nodes.

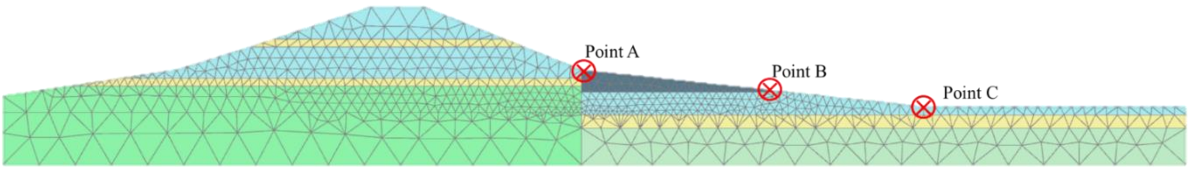

Fig. 3 Finite element mesh of the representative cross-section (Station 74 + 00)

To simulate the cyclic hydraulic loading acting on the levee, appropriate initial and boundary conditions were defined based on site conditions and the projected flood scenarios. The specific conditions applied in this study are summarized in Table 2. The analysis commenced with a steady-state simulation to establish the initial stress state and pore water pressure distribution. For this purpose, the initial river water level was set at EL. 5.4 m, representing the typical normal stage of the Tar River. This setup ensures the formation of a stable initial phreatic surface within the levee body prior to the application of transient flood loading.

Table 2 Summary of initial condition, boundary conditions, and cyclic hydraulic loading

Category	Boundary / Parameter	Condition / Value
Initial Condition	Initial Water Level	Constant head at EL. 5.4 m
Boundary Condition	Bottom and Sides	Impermeable boundaries
	Landside Slope	Seepage face
	Riverside Slope	Time-dependent total head
Hydraulic Loading	Cycle Duration	20 days (Rise : 3 days, Peak : 1 day, Drawdown : 3 days, Recovery : 13 days)
	Repetition	15 Cycles (300 days)

Following the initialization, boundary conditions were imposed to capture the hydraulic loading process. For the hydraulic domain, the bottom and vertical side boundaries were treated as impermeable surfaces. On the landside slope, a seepage face condition was imposed to allow water exfiltration only when the pore water pressure exceeded atmospheric pressure. Conversely, the riverside slope was subjected to a time-dependent total head boundary to simulate the flood hydrograph.

This transient hydraulic loading followed a 20-day period comprising four distinct phases. During the first phase, the water level increased from the initial elevation on Day 0 to a peak elevation of 8.0 m on Day 3, remaining at this peak until Day 4. This was followed by drawdown, during which the water level returned to the base elevation by Day 7. Subsequently, a recovery period maintained a constant water level until Day 20. This repetitive loading design was adopted to quantitatively evaluate the progressive accumulation of shear strain and the irreversible stiffness degradation over multiple flood events.

4. Results

This section presents the simulation results to evaluate the long-term stability of the levee under cyclic flood events. The analysis focuses on how water flow and soil deformation interact over time. First, the changes in pore water pressure and the movement of the phreatic line within the levee are examined. Next, the accumulation of shear strain at critical monitoring points is analyzed to identify structural vulnerabilities. Finally, the relationship between the conventional factor of safety and progressive plastic deformation is discussed.

4.1 Pore Water Pressure

Rapid fluctuations in river water levels induce significant changes in the internal seepage regime of a levee. These hydraulic variations alter the distribution of pore water pressure, thereby acting as a critical factor in governing local stability. To analyze the hydraulic responses under varying water levels, the evolution of pore water pressure and the expansion of the saturated zone were tracked at three stages: the initial (5.4 m), intermediate (6.8 m), and peak (8.0 m) conditions.

The analysis results indicate that as the river water level rises from the normal stage of 5.4 m to the flood stage of 8.0 m, the internal pore water pressure increases nonlinearly. Fig. 4 illustrates the distribution of pore water pressure and the variation of the phreatic line at different water levels. In the initial state (5.4 m), the phreatic line was stably formed at the lower portion of the levee (Fig. 4(a)). However, as the water level rose, the phreatic line gradually shifted upward, accompanied by a gradual transition of the internal unsaturated zone to a saturated state.

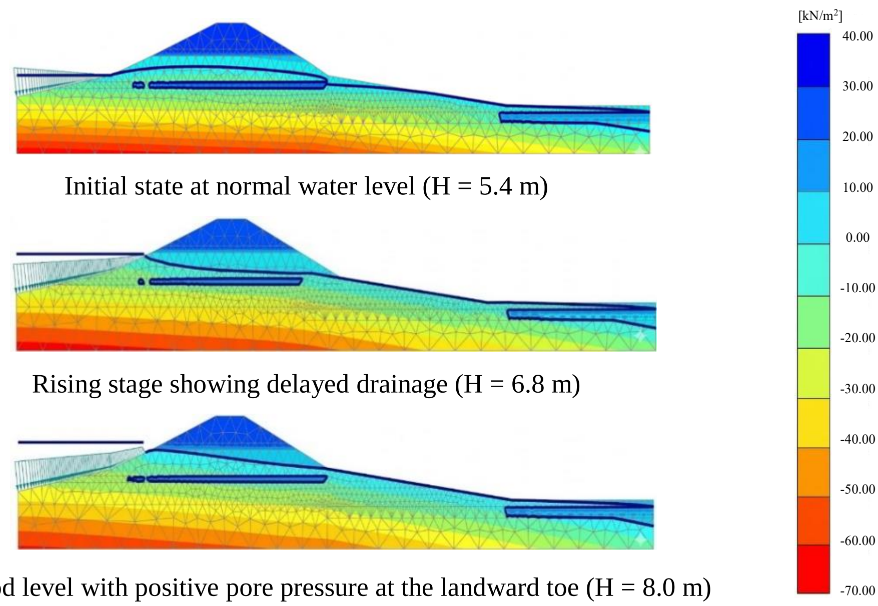

Fig. 4 Distribution of pore water pressure and variation of the phreatic line at different water levels

A notable hydraulic behavior was observed at the intermediate stage of 6.8 m (Fig. 4(b)). Although the levee interior had not yet reached full saturation, a delayed drainage was observed near the landward slope. This phenomenon is attributed to the low hydraulic conductivity of the SC and interbedded CL layers, which results in a time lag between the rapid external water level rise and the internal seepage velocity. This delayed drainage induces excess pore water pressure within the levee body and increases the hydraulic gradient, thereby heightening the potential for damage driven by seepage forces.

Furthermore, the discontinuous, rectangular strip-shaped pressure distribution observed in the central part of the levee body and the lower right foundation is associated with the interbedded low-permeability CL layers. While the surrounding high-permeability sandy layers (SC, SP) allow pore water pressure to propagate or dissipate rapidly, the aquitards (clay layers) require a relatively longer time to reach pressure equilibrium. Consequently, these layers exhibit an independent pore water pressure distribution that is distinct from the surrounding soil. This confirms that the numerical model successfully captures the stratification and the resulting hydraulic anisotropy of the actual ground.

When the water level reached its peak at 8.0 m (Fig. 4(c)), the saturated zone expanded across almost the entire cross-section. An important observation is the development of positive pore water pressure near the landward toe. Since soil shear strength is directly proportional to effective stress, the generation of positive pore pressure in this region leads to a reduction in effective stress, thereby weakening shear resistance. This finding suggests that the toe is a potentially vulnerable zone where piping or local sliding failure may develop under repeated flood conditions.

4.2 Deviatoric Shear Strain

Cyclic fluctuations in river water levels alter the internal stress state of the levee, inducing particle rearrangement and shear deformation within the soil mass. To evaluate deformation responses, the time-dependent variation of deviatoric shear strain was tracked at three critical locations on the landside slope, as illustrated in Fig. 3: the slope break (Point A), the mid-slope (Point B), and the landside bench (Point C). A comparative analysis indicates that Point A (slope break) exhibited the largest shear deformation, followed by the mid-slope (Point B) and the bench (Point C). Point A corresponds to a geometric inflection point where the levee crest intersects with the slope, resulting in localized stress concentration under increasing seepage pressure. This finding quantitatively identifies the slope break as the most critical section for potential failure initiation and suggests that it should be prioritized for monitoring during maintenance operations.

Fig. 5 presents the cumulative behavior of deviatoric shear strain at each monitoring point over 15 hydraulic cycles (N). A detailed analysis of the time-dependent deformation reveals a continuous upward trend in peak shear strain at all observation points. In the initial phase, a rapid increase in strain was observed, followed by a reduced rate of increase in later cycles. Despite this deceleration, the peak values continued to rise linearly. Specifically, over the course of 15 cycles, the peak shear strain at Point A increased by approximately 15% compared to the initial cycle. This demonstrates that the soil stiffness undergoes progressive degradation due to cyclic loading.

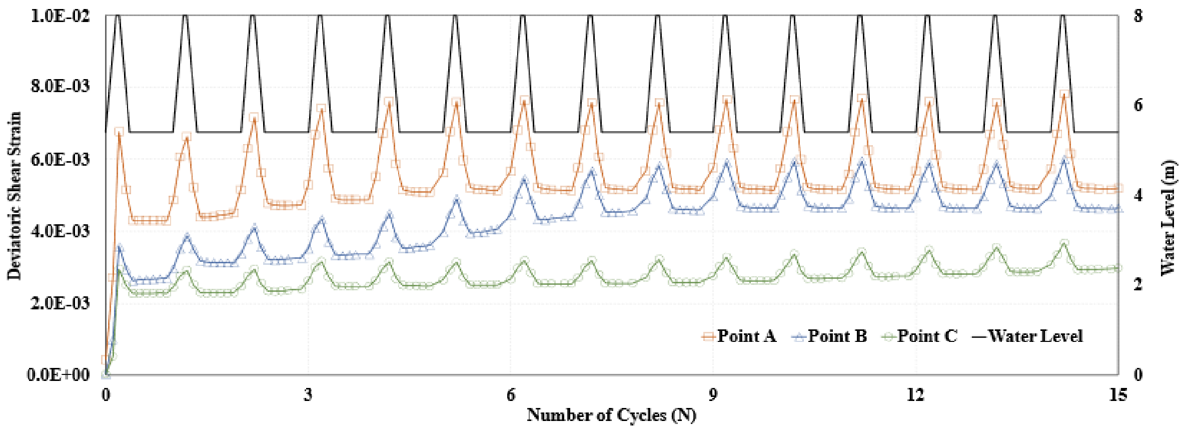

Fig. 5 Cumulative behavior of deviatoric shear strain at each point with increasing number of hydraulic cycles (N)

Additionally, a distinct baseline drift was observed in the strain time history. During the recovery phase, the shear strain did not fully revert to zero despite the recession of water levels, leaving a residual strain. This incomplete recovery accumulated with each subsequent cycle, resulting in a stepwise increase in the total deformation. Such behavior indicates that the plastic strains generated during the loading and unloading processes lead to permanent alterations in the levee geometry.

4.3 Analysis of Cyclic Shear Strain Behavior

The time-dependent evolution of deviatoric shear strain at critical locations (Points A, B, and C) provides quantitative insight into the cumulative deformation induced by cyclic hydraulic loading. Fig. 6(a) compares the peak shear strain evolution across these points. Point A (Slope break) exhibited the most significant accumulation, with the peak strain increasing by approximately 15% from the first to the fifteenth cycle. This accumulation pattern identifies the slope break as a geometric stress concentrator where hydro-mechanical fatigue is most pronounced.

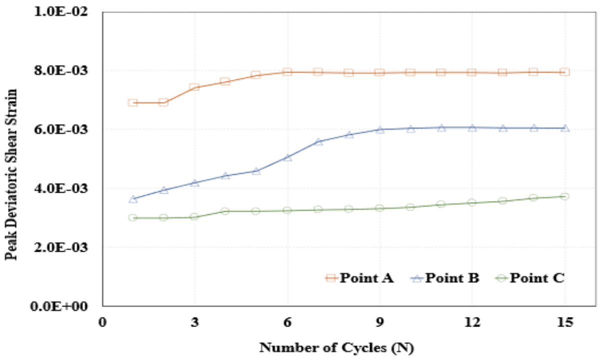

(a) Peak deviatoric shear strain evolution at monitoring points A, B, and C

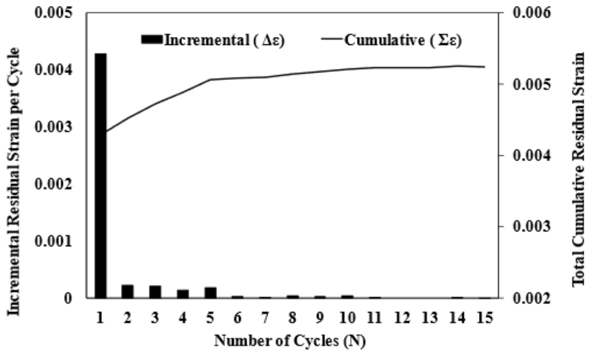

(b) Incremental and cumulative residual strain at Point A

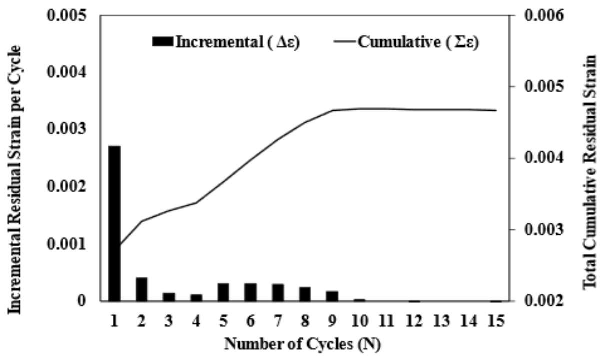

(c) Incremental and cumulative residual strain at Point B

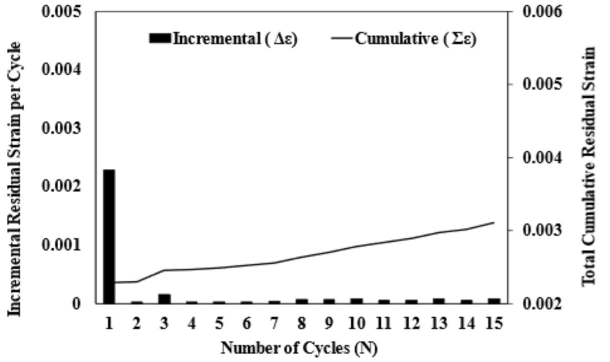

(d) Incremental and cumulative residual strain at Point C

Fig. 6 Time-dependent evolution of deviatoric shear strain and cumulative plastic deformation under cyclic hydraulic loading

A further observation is revealed by the dual-axis analysis of residual strain, as presented in Fig. 6(b)–(d). These figures contrast the incremental residual strain generated per cycle against the total cumulative residual strain. In the initial phase, a rapid accumulation of strain occurred due to primary densification and particle rearrangement. Subsequently, the incremental strain decreased significantly and converged toward a minimal value in the later cycles.

While this diminishing increment might suggest a stabilization of the soil structure, the cumulative strain curves demonstrate otherwise. The total deformation continues to exhibit a steady upward trend without reaching a plateau. This discrepancy indicates that the levee does not return to a purely elastic state but is consistent with a plastic shakedown or ratcheting regime. Although the plastic deformation added in each individual cycle becomes smaller, the continuous accumulation over the loading history results in a permanent alteration of the stress state. This phenomenon confirms that the shear strain generated during the high-water stage is not fully recovered during the unloading phase. Instead, the irreversible plastic component accumulates progressively, contributing to the stiffness degradation of the soil skeleton.

To quantitatively assess this stability, the global FoS was evaluated using the SRM at the most critical state after the 15th hydraulic cycle. The analysis yielded a global FoS of approximately 2.46. According to conventional design guidelines, such as the Korean River Design Standards, which mandate a minimum FoS of 1.3, this structure would be classified as highly stable against catastrophic failure [21].

However, this high ultimate FoS presents a critical paradox when contrasted with the time-dependent deformation behaviors observed in this study. Despite the mathematical assurance of macroscopic stability (FoS > 1.3), the local deviatoric shear strains continuously accumulate without full recovery during the drawdown phases. This indicates that the soil skeleton is undergoing progressive plastic yielding and irreversible stiffness degradation at the local response level.

Consequently, relying exclusively on a static limit equilibrium or a single ultimate FoS may lead to an overestimation of long-term levee performance. These findings strongly demonstrate that aging levees subjected to recurrent flood cycles should be evaluated through a deformation-based serviceability paradigm, where monitoring the threshold of unrecoverable plastic strain is far more crucial than simply satisfying a prescribed ultimate safety factor. Such an approach can provide a more realistic basis for long-term levee maintenance and risk management.

5. Conclusions

This study investigated the long-term hydro-mechanical response of the Princeville Levee under cyclic flood conditions through a fully coupled numerical analysis. By applying the hardening soil model, the research quantitatively evaluated the cumulative damage mechanism characterized by the interaction between transient seepage flow and soil stiffness degradation. The key findings and implications are summarized as follows:

(1) The hydraulic analysis revealed that the internal pore water pressure distribution is significantly governed by cyclic wetting and drying. Due to the low hydraulic conductivity of interbedded clay layers, a distinct delayed drainage phenomenon occurred. This hydraulic lag prevented the complete dissipation of pore water pressure during drawdown, leading to residual pore pressure accumulation that hindered effective stress recovery.

(2) The evolution of deviatoric shear strain demonstrated progressive mechanical degradation. Over 15 hydraulic cycles, peak shear strain increased continuously by 15% at the landside slope break. A dual-axis analysis highlighted that while the incremental strain per cycle diminished, the total cumulative residual strain rose steadily. This ratcheting behavior indicates that the soil undergoes irreversible plastic deformation rather than reaching an elastic shakedown state.

(3) The slope break was identified as the most critical vulnerability zone. The geometric discontinuity of this section acts as a stress concentrator where high shear strain accumulation and residual pore pressure are most pronounced. Consequently, safety monitoring protocols should prioritize the slope break area to detect early signs of progressive failure.

(4) The strength reduction method evaluated the global factor of safety at 2.46 after 15 cycles. While this macroscopic metric comfortably exceeds conventional design standards, a notable discrepancy emerges when it is contrasted with the observed strain ratcheting. This finding demonstrates that traditional static assessments relying solely on ultimate safety factors may overestimate long-term levee integrity by overlooking cumulative internal damage.

Future research should extend the present framework by incorporating these numerical findings into the development of a standardized stability assessment methodology for aging levees. Specifically, the relationship between cumulative hydraulic degradation and effective stress recovery identified in this study will be utilized to propose a more rigorous, deformation-based seepage stability evaluation protocol.

Acknowledgments

This work was supported by Korea Environment Industry & Technology Institute (KEITI) through Research and development on the technology for securing the water resources stability in response to future change Project, funded by Korea Ministry of Climate, Energy and Environment (MCEE) (RS-2024-00332877).

Conflicts of Interest

The authors declare no conflict of interest.

References

[1] I. E. Özer, M. van Damme, and S. N. Jonkman, “Towards an International Levee Performance Database (ILPD) and Its Use for Macro-Scale Analysis of Levee Breaches and Failures,” Water, vol. 12, no. 1, article no. 119, 2019.

[2] D. K. Im, H. K. Yeo, K. H. Kim, and J. G. Kang, “A Study on the Suitability of the Numerical Model for the Seepage Analysis in the Levee,” Journal of Korea Water Resources Association, vol. 39, no. 3, pp. 241-252, 2006. (in Korean)

[3] M. C. Park, J. W. Lee, Y. S. Kim, and H. S. Han, “Seepage Analysis of Large Scale Levee Model Using Improved TDR Sensors,” Journal of the Korean Geotechnical Society, vol. 28, no. 11, pp. 53-67, 2012. (in Korean)

[4] S. W. Jin, Y. W. Choo, Y. M. Kim, D. S. Kim, and E. S. Im, “Seepage Behavior of Reinforced Levee on Low Permeability Foundation Using Centrifuge Model Test,” Journal of the Korean Geotechnical Society, vol. 28, no. 5, pp. 27-39, 2012. (in Korean)

[5] M. D. Sleep, “Analysis of Transient Seepage Through Levees,” Ph.D. dissertation, Virginia Polytechnic Institute and State University, Blacksburg, VA, USA, 2011.

[6] W. C. Huang, M. C. Weng, and R. K. Chen, “Levee Failure Mechanisms during the Extreme Rainfall Event: A Case Study in Southern Taiwan, Natural Hazards, vol. 70, pp. 1287-1307, 2014.

[7] N. Rossi, M. Bačić, M. S. Kovačević, and L. Librić, “Development of Fragility Curves for Piping and Slope Stability of River Levees,” Water, vol. 13, no. 5, article no. 738, 2021.

[8] A. Semerci, G. Tayfur, and H. F. Pulat, “Numerical Modelling of Flood Induced Seepage Under Levees,” European Journal of Science and Technology, no. 27, pp. 495-507, 2021.

[9] S. E. Cho, “Probabilistic Stability Analysis of Earthen Levees Considering the Hydraulic and Mechanical Properties of Soil,” Journal of the Korean Geotechnical Society, vol. 41, no. 1, pp. 55-68, 2025. (in Korean)

[10] A. Shivamanth, S. S. Athani, M. K. Desai, and G. R. Dodagoudar, “Stability Analysis of Dyke Using Limit Equilibrium and Finite Element Methods,” Aquatic Procedia, vol. 4, pp. 884-891, 2015.

[11] B. M. Montoya and V. Bennett, “Deformation Based versus Limit Equilibrium Analyses to Assess the Effect of Repeated Rise and Fall of Water Level on the Stability of Princeville Levee”, Association of State Dam Safety Officials, Technical Report, 2018.

[12] R. Jadid, B. M. Montoya, V. Bennett, and M. A. Gabr, “Effect of Repeated Rise and Fall of Water Level on Seepage-Induced Deformation and Related Stability Analysis of Princeville Levee,” Engineering Geology, vol. 266, article no. 105458, 2020.

[13] A. Vreeland, “Hazard Mitigation Strategy Application: An Evaluation of the Town of Princeville’s Future Mitigation Strategies,” Master’s dissertation, University of North Carolina at Chapel Hill, 2019.

[14] Y. Sun, Z. Li, K. Yang, G. Wang, and R. Hu, “Analysis of the Influence of Water Level Change on the Seepage Field and Stability of a Slope Based on a Numerical Simulation Method,” Water, vol. 15, no. 2, article no. 216, 2023.

[15] J. H. Kim, Y. M. Kim, and A. Satyanaga, “Instability of Embankment Slopes Due to Overflow and Drawdown,” Water, vol. 15, no. 19, article no. 3402, 2023.

[16] D. Janssen, D. P. Hommes, A. J. M. Schmets, B. Hofland, C. Zwanenburg, E. Dado, et al., “Experimental Study of Water Infiltration into a Partially Sealed Levee,” Journal of Geotechnical and Geoenvironmental Engineering, vol. 151, no. 1, 2025.

[17] US Army Corps of Engineers (USACE), “Princeville, North Carolina, Flood Risk Management: Integrated Feasibility Report and Environmental Assessment,” USACE Wilmington District, Technical Report, 2015.

[18] R. F. Carsel and R. S. Parrish, “Developing Joint Probability Distributions of Soil Water Retention Characteristics,” Water Resources Research, vol. 24, no. 5, pp. 755-769, 1988.

[19] T. Schanz, P. A. Vermeer, and P. G. Bonnier, The Hardening Soil Model: Formulation and Verification, in Beyond 2000 in Computational Geotechnics, London, UK: Taylor & Francis, pp. 281-296, 1999.

[20] M. T. van Genuchten, “A Closed-Form Equation for Predicting the Hydraulic Conductivity of Unsaturated Soils,” Soil Science Society of America Journal, vol. 44, no. 5, pp. 892-898, 1980.

[21] Korea Water Resources Association (KWRA), River Design Standard and Commentary, Korea Water Resources Association, 2019. (in Korean)